Hyperpolarised gas filling station for medical imaging using polarised ^{129}Xe and ^{3}He

Lee, Wai Tung; Zheng, Gang; Talbot, Cavin L.; Tong, Xin; D'Adam, Tim; Parnell, Steven R.; de Veer, Michael; Jenkin, Graham; Polglase, Graeme R.; More Authors

DOI
10.1016/j.mri.2021.02.010

Publication date
2021

Document Version
Final published version

Published in
Magnetic Resonance Imaging

Magnetic Resonance Imaging 79 (2021) 112–120

Contents lists available at ScienceDirect

Magnetic Resonance Imaging

journal homepage: www.elsevier.com/locate/mri

Technical Note

Hyperpolarised gas filling station for medical imaging using polarised ^{129}Xe and ^{3}He

Wai Tung Lee [a,1,*], Gang Zheng [b], Cavin L. Talbot [c], Xin Tong [d,e], Tim D'Adam [a], Steven R. Parnell [f], Michael de Veer [b], Graham Jenkin [g], Graeme R. Polglase [g,h], Stuart B. Hooper [g,h], Bruce R. Thompson [i], Francis Thien [j], Gary F. Egan [b]

[a] Australia Nuclear Science and Technology Organization, Lucas Heights, New South Wales 2234, Australia
[b] Monash Biomedical Imaging, Monash University, Melbourne, Victoria 3800, Australia
[c] University of Queensland, St Lucia, Queensland 4072, Australia
[d] Spallation Neutron Source Science Center, Dongguan, 523803, China
[e] Institute of High Energy Physics, Chinese Academy of Sciences, Beijing 100049, China
[f] Delft University of Technology, Mekelweg 15, 2629 JB, Delft, the Netherlands
[g] The Ritchie Centre, Monash University and Hudson Institute of Medical Research, Clayton, Victoria 3168, Australia
[h] Department of Obstetrics and Gynaecology, Monash University, Clayton, Victoria 3168, Australia
[i] Swinburne University of Technology, Hawthorne, Victoria 3122, Australia
[j] Eastern Health Clinical School, Monash University, Clayton, Victoria 3168, Australia

ARTICLE INFO

Keywords:
Hyperpolariser
Hyperpolarised Xenon-129
Hyperpolarised Helium-3
MRI lung imaging: Spin-exchange optical pumping

ABSTRACT

We report the design, construction, and initial tests of a hyperpolariser to produce polarised ^{129}Xe and ^{3}He gas for medical imaging of the lung. The hyperpolariser uses the Spin-Exchange Optical Pumping method to polarise the nuclear spins of the isotopic gas. Batch mode operation was chosen for the design to produce polarised ^{129}Xe and polarised ^{3}He. Two-side pumping, electrical heating and a piston to transfer the polarised gas were some of the implemented techniques that are not commonly used in hyperpolariser designs. We have carried out magnetic resonance imaging experiments demonstrating that the ^{3}He and ^{129}Xe polarisation reached were sufficient for imaging, in particular for in vivo lung imaging using ^{129}Xe. Further improvements to the hyperpolariser have also been discussed.

1. Introduction

1.1. Magnetic Resonance Imaging (MRI) of the lung

In the year 2020, severe acute respiratory syndrome coronavirus-2 (SARS-CoV-2) pandemic caused a serious global health crisis. SARS-CoV-2 not only has a high mortality rate [1] but also long-term effects especially in lung [2]. However, there is still a lack of methods in dealing with these potential chronic effects. Magnetic resonance imaging (MRI) is one of the most important tools for diagnosis because of its unique contrast of protons in tissues. However, MR imaging of the lung is difficult because its low proton density and is further complicated by the many air-tissue interfaces that cause magnetic susceptibility artefacts and a rapid decay of the MR signals in lung. The use of hyperpolarised isotopic gases ^{3}He and ^{129}Xe has revolutionised MR lung imaging and opened up the important new research field of functional lung imaging.

Hyperpolarised gases belong to a new class of inhaled contrast agents and can be used to achieve high spatial-temporal resolution MR images of lung. These gases are able to increase the MR signals by approximately 10,000 times compared with that from a sample in thermal equilibrium [3]. The first hyperpolarised gas MR image was reported nearly three decades ago in a mouse lung using ^{129}Xe [4], and in human lungs using ^{3}He two years later [5].

1.2. Spin-exchange optical pumping production of hyperpolarised ^{129}Xe and ^{3}He gases

Hyperpolarised gas can be produced using a hyperpolariser based on

* Corresponding author.
E-mail address: waitung.lee@ess.eu (W.T. Lee).
[1] Current affiliation: European Spallation Source, Lund 224 84, Sweden.

https://doi.org/10.1016/j.mri.2021.02.010
Received 30 September 2020; Received in revised form 12 February 2021; Accepted 12 February 2021
Available online 15 February 2021

a process called Spin-Exchange Optical Pumping (SEOP) [6,7]. The SEOP process to achieve nuclear polarisation is a three-step process: optical pumping, collisional spin-exchange and hyperfine interaction. In a typical arrangement, the centre piece is a glass cell (optical pumping cell, or "OPC" in short) containing a mixture of either ^{129}Xe gas or ^{3}He isotopic gas, nitrogen and vapour of alkali, either rubidium, potassium, or a selected mixture of both. Circularly polarised laser light with wavelength set to the D1 transition line of the alkali illuminates the mixture. The circular polarisation of the light results in the optical pumping process selectively exciting alkali atoms in one of the two spin-states of the ground state $^{2}S_{1/2}$ to the $^{2}P_{1/2}$ excited state. Subsequent decay of the excited state induced by collisions or spontaneous emission returns the excited atom to the ground state. This sees a majority of the excited atoms re-populate equally the two spin-states of the ground state. Since the circularly polarised laser light selectively pumps one spin-state, the alkali vapour reaches a high polarisation in the spin state that has not been optically pumped.

In the next step, spin-exchange between an alkali atom and a noble gas atom occurs when the two collide. This process transfers the polarisation of the alkali atom to the noble gas atom. In the final step, hyperfine interaction further transfers the atomic polarisation to the nuclei of the noble gas. As the alkali-noble gas spin-exchange collision has a relatively low cross-section, a majority of the polarising time is spent on waiting for enough spin-exchange to occur. It takes minutes for ^{129}Xe to reach high polarisation and it takes many hours or days for ^{3}He. The physics of SEOP has been studied extensively. These studies have informed selection of the parameters of a hyperpolariser.

1.3. Motivation and selection of the hyperpolariser characteristics

In earlier lung ventilation MRI experiments conducted on an MRI scanner in Melbourne, Australia, hyperpolarised ^{3}He gas stored in a GE-180 glass cell was transported in a uniform magnetic field container from a production facility in Mainz, Germany. The journey took more than 30 h. Due to the polarisation lifetime (the exponential decay time-constant is commonly referred to as "T1") between 80 and 130 h in the transporter, there was sufficient preservation of the polarisation for experiments [8]. In fact, the closest hyperpolariser to Melbourne at the time was in Japan, which takes 15-h flight time. The carefully choreographed transportation process worked to establish MRI hyperpolarised gas lung imaging research in Melbourne. However, it was virtually impossible to transport ^{129}Xe over similar distances. The T1 of hyperpolarised ^{129}Xe in a uniform magnetic field of up to several Tesla is less than 10 h. In a viable transporter that keeps frozen xenon in a glass vessel inside a Halbach cylinder at up to several hundred mT, the ^{129}Xe polarisation would have a T1 of a few hours. Therefore, to establish a local production capability for hyperpolarised gases for MRI, we carried out a project to design and construct a hyperpolariser. The project goal was to construct a hyperpolariser and demonstrate that MRI imaging with polarised ^{129}Xe and polarised ^{3}He could be achieved.

The first design choice was whether to use Spin-Exchange Optical Pumping (SEOP) or Metastable Exchange Optical Pumping (MEOP) [9]. At present, MEOP systems can polarise ^{3}He while SEOP systems can polarise both ^{129}Xe and ^{3}He. At the Monash Biomedical Imaging centre where the hyperpolariser is located, a 3-Tesla MRI scanner was upgraded for ^{129}Xe imaging. The hyperpolariser is within a two-minute walk to the 3 T scanner and a second MRI scanner for polarised ^{3}He imaging as discussed above is located within a one-hour drive. We therefore aimed to provide both polarised ^{129}Xe and polarised ^{3}He and consequently decided to use SEOP.

The next decision was a choice between using batch mode setup and using continuous gas-flow mode setup. In batch mode setup to polarise either ^{129}Xe or ^{3}He, the operations to polarise either gas are similar. The main differences are (1) the combination of the gas species, (2) the polarising temperature between 60 °C to 100 °C for ^{129}Xe and between 160 °C to 200 °C for ^{3}He, and (3) polarised ^{3}He gas needs to be cooled down before extraction. Conventional gas-flow mode is well-suited for hyperpolarised ^{129}Xe production, especially in conjunction with a cryogenic setup using liquid-nitrogen cold-trap to freeze and collect the ^{129}Xe in large dose. Freezing polarised ^{129}Xe also increases its polarisation lifetime to allow several cycles of production. Storage and transportation in a high magnetic field would further extend the ^{129}Xe polarisation lifetime. A Halbach cylinder provides up to several hundred mT and is often used together with a cryogenic setup. This method works well also in part because the time to polarise ^{129}Xe is usually measured in minutes. In contrast, at least half-a-day is usually required to polarise ^{3}He. The shortest "pump-up" time-constant reported at the time was close to five hours [10], meaning that it would reach about 2/3 of the maximum polarisation in that time. Thus, polarised ^{3}He production would have a lower benefit from continuous-flow operation. A continuous flow hyperpolariser can in principle be designed to also operate in a stop flow/batch mode to polarise ^{3}He [11,12]. A technical complexity in realising such a hyperpolariser is related to the relatively high polarising temperature of ^{3}He. Care must also be taken to ensure the stop-flow mechanism does not reduce the polarisation and furthermore the design would involve considerable R&D efforts to develop. As our focus was on the production of a hyperpolariser within the constraints of a reasonable time and the available resources to demonstrate successful operation with MRI measurements, we opted for a batch mode design.

For the production of hyperpolarised ^{129}Xe, a setup to freeze xenon in a Halbach cylinder would be advantageous to have but the mechanism to freeze and thaw xenon, and the field uniformity and the prevention of depolarisation due to zero-field-crossing along the flow path needs time and effort to develop. Transporters with 1.2 mT uniform magnetic field were available to us. Although the polarisation lifetime is only ten to twenty minutes for polarised ^{129}Xe in gaseous state at this field strength, the hyperpolariser location is within two-minute walk to the 3 T scanner with ^{129}Xe MRI setup. Therefore, we focused on construction of the hyperpolariser and application to the initial MRI imaging measurements as reported here, with improvements in the collection and transportation device to be undertaken at a later stage.

In relation to the characteristics of SEOP and noble gas polarisation, there have also been advances in a number of hyperpolariser technologies that have yet to be adopted in hyperpolarisers manufactured for medical imaging applications. Some of these technologies are two-side pumping, electrical heating, a piston to transfer the polarised gas and incorporation of the recycling and purification setup into the gas circuit. In this report, we provide further details on their adaptation, together with details of the optical pumping cell, oven, magnetic field coils and automation. Our work is consistent with the decades of continuous advancement of hyperpolariser technology carried out by many groups.

2. Materials and methods

The hyperpolariser consists of six major parts (Fig. 1): an optical pumping cell, cell temperature control oven, laser optics, uniform magnetic field coils, gas circuit and automation. In addition, an auxiliary gas-transporter to transport polarised gas to the MRI scanner is include in the suit of equipment. In order to supply polarised ^{129}Xe and polarised ^{3}He, batch mode operation was chosen for the hyperpolariser. In addition to being able to polarise both types of gas isotopes, batch mode has more flexibility for the control of the alkali vapour pressure and the polarisation time required to optimise the performance of the hyperpolariser. In a departure from existing hyperpolariser designs, we used two-side pumping method, electric heating and a piston gas driver to extract the polarised gas from the optical pumping cell.

2.1. Optical pumping cell

The optical pumping cell was fabricated from GE-180 alumina silicate glass (Fig. 2). The glass was originally developed by General Electric for use with sodium lamps. It can sustain the presence of alkali at

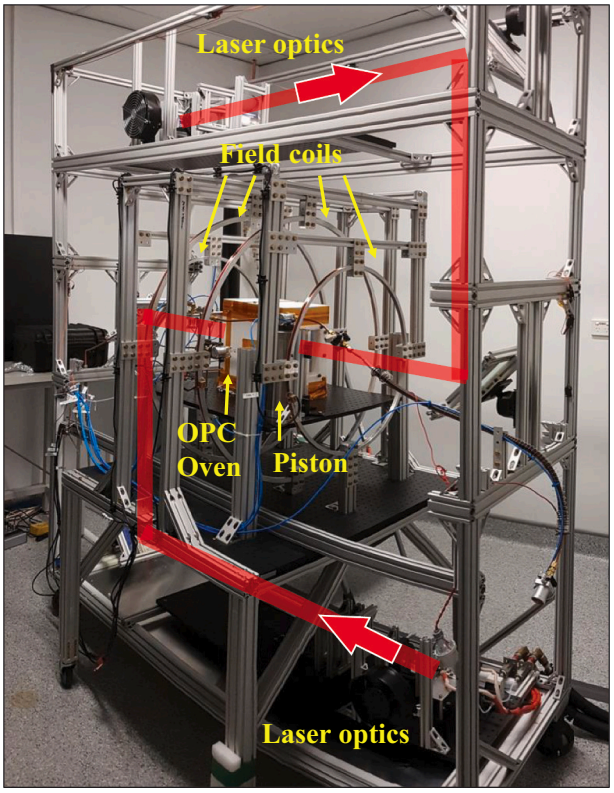

Fig. 1. Overview of the polariser showing some of the major subsystems: Oven with OPC inside, Laser optics, field coils and laser optics. The laser pathway is illustrated in red.

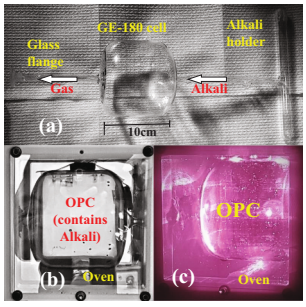

Fig. 2. Optical pumping cell. (a) GE-180 cell body with custom Pyrex flange and alkali distillation arm. (b) Completed OPC in the oven after alkali has been distilled into the cell body and the distillation arm dismounted. The Free-Induction Decay NMR coils are shown. (c) Laser light shined on the OPC during SEOP process to produce hyperpolarised xenon-129 gas

elevated temperature whereas other types of glass would be corroded and become opaque [13]. In addition, a blown GE-180 cell was found to be less porous, potentially reducing the wall-relaxation that depolarises the gas [14]. The glass cell has 120 mm ID and 80 mm inner length, and a volume of 0.9 l. A borosilicate glass flange was welded to the circular end of the cell to provide gas passage. The glass flange was custom-made with 2 mm ID passage from end to end to reduce the "dead volume" where the gas is not polarised. An additional capillary was welded onto the cell to prepare for the distillation of alkali into the cell.

A pneumatically actuated valve was mounted onto the glass flange to contain the gas during the polarising process. The valve uses a 5 mm diameter FFKM perfluoroelastomer ball (Dupont Kalrez®) to plug the opening of the glass valve. Retracing the Kalrez® ball allows the gas to flow through a channel in the valve. An additional Kalrez® O-ring sealed the space from the flange to the valve. While the valve is outside the high-temperature region, Kalrez® was chosen for its high-temperature stability up to 327 °C and for its chemical inertness. The body of the valve was made entirely from either grade-2 titanium or aluminium. We chose these materials instead of stainless steel to avoid residual magnetism commonly found on machined stainless steel components, which would depolarise the gas. Polarised gases during transfer from the optical pumping cell to a transport cell pass about 40 mm of the valve material. Our previous tests have shown no degradation of gas polarisation with either type of valves.

After fabrication the cell body was repeatedly rinsed with filtered soapy water followed by sterile filtered water. Clean nitrogen gas was flowed through the cell to remove the water while preventing contaminants from entering. The pneumatic valve was attached and an ampoule containing 1 g of alkali, in our case rubidium, was sealed into the capillary. Through the opened valve, the cell was pumped by a turbomolecular pump while baked at 450 °C. Both the valve and the ampoule of alkali remained outside the oven. Residual Gas Analyser was used to monitor the level of water until its partial pressure dropped to 2×10^{-6} mbar, after which the baking ceased and the assembly cooled to room temperature. While still attached to the vacuum pump, the alkali was heated by a heat gun and distilled into the cell. Finally, the capillary was closed by a flame torch at a location close to the cell and the remaining capillary and ampoule were removed.

2.2. Cell temperature control oven

The degree to which ^{3}He gas is polarised and the pump-up rate depends on the alkali vapour density which in turn depends on the OPC temperature and the laser heating effect, and the photon density available for optical pumping [15]. For ^{129}Xe gas, the rate also depends on the gas mixture [16]. Such dependencies have been mapped out extensively [17].

At room temperature, the vapour pressure of the alkali is too low to be effective. The optical pumping cell is therefore placed in an oven to control the temperature. The oven walls were made from virgin grade Teflon® sheets to provide the insulation. Double-pane glass windows at the two sides were covered with anti-reflective coatings to allow the laser light to reach the OPC.

Conventionally, heating is done by flowing pre-heated air into the oven. The drawback is that large quantities of hot air are constantly vented from the hyperpolariser. We have instead adopted electric heating [18] to reduce heating the ambient environment. To prevent magnetic interference, a heater pad with a "non-inductive" wiring pattern was used. The heater pad was placed 90 mm below the cell and driven by a DC power supply.

Without air flow, a temperature gradient may develop in the oven. When polarising ^{129}Xe, air flow from a compressed air supply at a rate less than 10 cc/min is introduced from the top of the oven to induce convection. The temperature inside the oven is monitored by two RTD temperature sensors. One sensor is placed on the inside of the top lid at 40 mm above the top of the cell. The other sensor is placed underneath an opaque Teflon cell-support bar at 20 mm below the bottom of the cell and 30 mm above the heater pad. The sensors are outside the volume illuminated by the laser beam so as to avoid erroneous temperature readings due to laser heating. The temperature readings are typically within 1 °C of each other. In fact, we found little thermal gradient after shutting off the air flow when polarising ^{129}Xe at temperatures between 80 °C and 100 °C. When polarising ^{3}He between 180 °C to 200 °C, about 10 cc/min air flow achieved the same thermal uniformity. A further improvement may be the use of a piezoelectric fan inside the oven to circulate the air inside the cell rather than by introducing external air flow through the oven.

2.3. Laser optics

Narrow bandwidth solid-state lasers with volume Bragg grating (VBG) attached have in recent years replaced the large array of optics of an external Lithrow cavity [19]. In our setup, we use 794.7 nm (in air) lasers with VBG narrowed bandwidth of 0.3–0.4 nm. Each laser stack consists of four lines of 60 W laser and each emission line has a VBG built in. A temperature regulated distilled water flow at 1.3–1.5 lpm is used to cool and control the temperature of the laser. With the VBG built-in, the layout and operation of the laser optics is highly simplified (Fig. 3). Optics were used first to collimate the fast-axis which has a 36° divergence. The linearly polarised laser light then passes through a polarising beam splitter to ensure the laser going downstream has virtually no elliptical component. A quarter-wave plate then changes the laser to circularly polarised. A fan is used to keep the waveplate and the beam splitter cool as a precaution. The rest of the optics are cylindrical lenses to shape the laser beam profile in order to have a highly parallel beam that fully illuminates the OPC but not illuminating the oven body. The laser light needs to be parallel to the applied magnetic field in order to be most effective in the optical pumping process.

The system geometry uses "side-pumping" with the laser entering the cell from the cylindrical side. In addition, most if not all hyperpolarisers for medical imaging use single-side pumping with the laser coming from one direction only. We instead use a two-side pumping scheme: two laser beams enter from opposing side of the OPC. Our previous experience has shown that two-side pumping in batch mode operation results in higher polarisation. We believe this is related to lensing – the directional change of the laser light by the glass wall. The curvature of the glass cell causes the laser to deviate from being parallel to the magnetic field. This can be corrected by optics. There are however also variations of the glass thickness in the cell wall that result in non-uniform redistribution of the laser intensity, which is virtually impossible to correct. In this situation, two-side pumping may allow a more even distribution of laser light throughout the cell volume, as it is unlikely the lensing from both side of the cell results in depleted laser intensity in the same region, thereby improving the polarisation. We performed single-sided pumping and found the FID signal at the MRI to be lower by as much as 30% compared to the signal from using two-side pumping. This comparison is possible as the precise climate controlled environment in the MR room and the repeatable setup allow the FID signal measurements to be reproducible. Such effects have been reported by different groups and different mitigation methods have been tested. In one report, researchers used a mirror downstream from the OPC to retro-reflect the laser back towards the OPC, which increased the polarisation level to about 29% (see, e.g. reference [16]). The OPC used in our system is a blown cell and variations in the glass thickness were visible. Whilst there is the possibility that the lensing effect could be compounded when using a retro-reflective mirror, the efficiency of the two-side pumping scheme justifies further investigation.

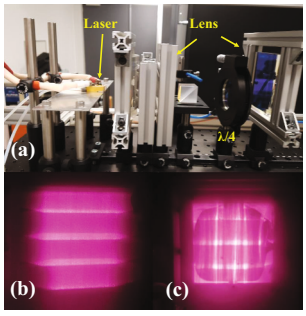

Fig. 3. Laser optics. (a) One of the two setups: The laser is a 4x60W stack with Volume Bragg Grating built-in to narrow the bandwidth, a quarter-waveplate to produce circular polarisation of the laser light, and lenses to shape the beam profile to cover the optical pumping cell. (b) Laser profile at the entrance of the oven. (c) Projected laser profile after the OPC. The vertical streaks are due to lensing by the uneven glass wall of the blown Ge-180 cell.

The two lasers are mounted on platforms above and below the optical pumping cell, respectively. Custom-made dielectric polarisation-preserving mirrors with 99% reflectivity at 45° reflect the laser beam from the beam-shaping optics towards the OPC. This arrangement doubles the optical path to achieve a parallel beam without increasing the footprint of the hyperpolariser. The anti-reflective coating on an optical element has 99.75% transmission. 80% of the laser beam that enters the oven is delivered to the OPC due to the mismatch of the laser beam and the OPC cross-sectional profiles. Counting the number of optical elements, we estimated that 75% of the 480 W total power of the lasers, or 360 W has been delivered to the OPC.

2.4. Magnetic field coils

There are three causes of gas depolarisation: dipole-dipole interactions between nuclei in close proximity of each other, wall-relaxation at the inner cell walls, and magnetic field inhomogeneity. A highly uniform magnetic field covering the OPC is crucial for gas polarisation. In our setup, a "tetracoil" [20] was used to provide a uniform field (see Fig. 1). The tetracoil achieves a high uniformity within the OPC cell volume with field gradient $|\nabla B_{\perp}/B| < 10^{-4}$/cm, where $B_{\perp}$ is the field component transverse to the main field direction parallel to the coil axis. The field magnitude was set to 1mT. Compared to a Helmholtz coil of similar size, the uniformity volume of a tetracoil is more than three times larger, and whilst there are other coil systems with similar uniformity volume the tetracoil is the most compact system.

In the initial setup, a mu-metal shielded, compensated rectangular solenoid was used to provide the uniform field. However, despite the initial good performance, the size and shape of the mu-metal shielding began to deform under its own weight and due to the stress of thermal cycling. During the first two years of operation the decay time of the free-induction decay signal, a measure of the magnetic field uniformity, has reduced from 180 ms to 50 ms. Measurements using a three-dimensional fluxgate that is sensitive to 10^{-4} mT has also shown a degradation of the field uniformity compared to similar measurements when the solenoid was just installed.

2.5. Gas circuit

2.5.1. Structure and operation

The gas circuit regulates the combination of noble gas and nitrogen for each production batch of polarised gas (Fig. 4). The centre line of the gas circuit connects the gas supply bottles, the OPC, the gas-transfer piston, the transport cell and the vacuum pumps. An inline gas purifier removes contaminants including water, oxygen, carbon dioxide and hydrocarbons down to the level of parts per billion before the gas enters the OPC. An inline pressure gauge monitors the gas pressure, providing feedback to the control program. A Residual Gas Analyser (RGA) attached to a turbomolecular pump measures the level of contaminants. Using sequences of timed opening and closing of the pneumatic valves, the gas circuit supplies the selected combination of noble gas and nitrogen to the OPC, transfers polarised gas through the piston to a transport cell or a Tedlar bag, performs nitrogen purges to clean the gas lines, and pumps out unwanted gas species.

A titanium based pneumatically driven piston is used as an intermediate step in transferring polarised gas. The piston uses two Fluorocarbon (Viton) o-rings for sealing, which were vacuum-baked to outgas before installation. Krytox™ low vapour pressure lubricant was used. The piston is driven by a pneumatically driven actuator. This is adapted from MEOP based hyperpolariser technology. In a MEOP system, tens of mbars of polarised ^{3}He gas is drawn from the OPC and compressed into an intermediate holding cell by a similarly constructed but larger size Titanium piston [21]. The process repeats until the holding cell reaches 0.1 to 0.3 bars of gas. Then the polarised gas is drawn back to the piston

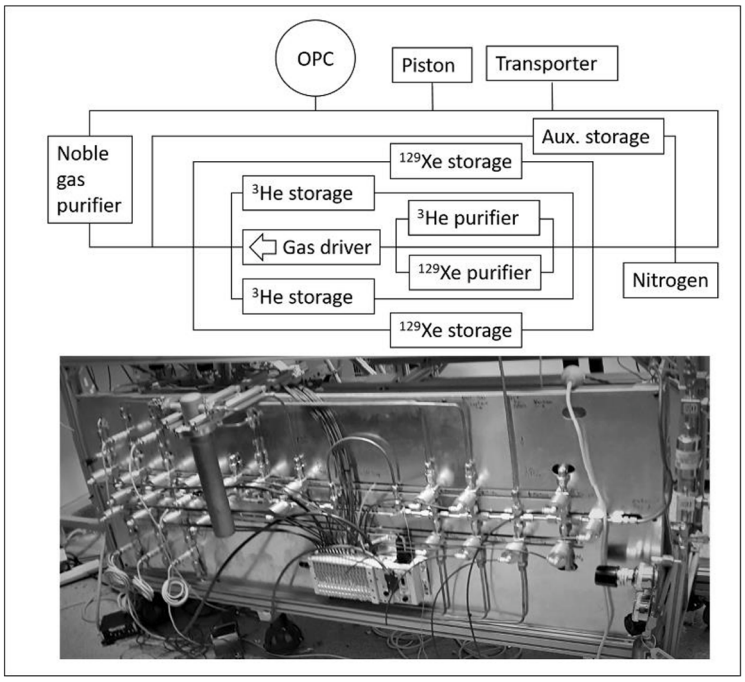

Fig. 4. (top) Gas circuit connection schematics. The valves that control the gas flow are not shown. (bottom) Gas circuit and controller.

and transferred from the piston to a transport cell. These steps are repeated until the required amount of gas in the transport cell is reached.

In our setup, the polarised gas first flows into the piston before being transferred from the piston to a transport container. This procedure avoids accidentally exposing the OPC to air, for instance, due to a punctured Tedlar bag. Upon each gas transfer from the piston, the remaining gas in the circuit is recycled, followed by rapid nitrogen purging of the circuit. By repeating the transfer procedure, more polarised gas is transferred. To prevent back flow, the piston compresses the polarised gas before a valve is opened to flow the gas to the transport container.

Compare to the piston used in MEOP, the compression ratio requirement is lower for the piston in our hyperpolariser as we do not need to extracted and compressed low-pressure gas. Our piston is actuated several times to transfer most of the polarised gas from the OPC. As we designed the OPC and piston to have similar sizes, a total of two strokes of the piston would transfer 3/4 of the polarised gas and three strokes would transfer 7/8 of the polarised gas. An identical piston was tested in a different laboratory with polarised ^{3}He. The fractional polarisation-loss was well below 0.01, i.e. for ^{3}He gas with 70% polarisation, each stroke cycle of the piston to draw in and expel gas would reduce the gas polarisation by less than 0.01 × 70%.

2.5.2. Recycling and purification

Isotopic ^{129}Xe and ^{3}He gases are expensive. A percentage of the noble gas can be recovered after performing medical imaging. The recovered gas needs to be purified to remove the water, oxygen and hydrocarbon to a level of parts per billion before it can be reused. Rather than purifying the gas in a separate instrument, we have integrated recycling and purification capabilities into the gas circuit.

To purify xenon, the mixed gas recovered from an experiment flows multiple times between two storage bottles through a cold trap cooled by liquid nitrogen. Xenon condenses on the surface of the cold trap. With most of the xenon condensed, the remaining gas is evacuated. The process removes oxygen, nitrogen and water, as these substances are gaseous in the sub-mbar vacuum at the 77 K liquid nitrogen temperature. After removing the unwanted gases, the cold trap temperature is raised by removing the liquid nitrogen. Xenon begins to evaporate at 120 K at low pressure and can be retrieved into the storage bottle while carbon dioxide remains a solid until 140 K. The two gases can be separated by monitoring the temperature of the warming cold trap.

To purify helium, the mixed gas flows through a different liquid nitrogen cold trap containing activated carbon. The cold activated carbon traps all other gas species except helium. After cycling a few times, the helium can be stored and the contaminants released by warming and pumping out the cold trap. To examine the purity of the xenon or helium gas, the gas can be cycled through the gas circuit from one storage bottle to another. The trace amount of remaining gas can be analysed by the RGA. The purification process can commerce until it reaches a satisfactory level of purity.

2.6. Automation

The choreography of gas flow, oven temperature, laser power, and polarisation monitoring is difficult to carry out by hand. A LabView program was written to handle the majority of the processes (Fig. 5). Several sub-programs were created, each carrying out a separate action: preparation of the OPC content, gradual energisation of the laser and setting the polarising temperature, preparation of the polarised gas transport bag or container, polarised gas transfer, etc. The program informs the hyperpolariser operator on the status of the processes, monitors physical quantities such as Free Induction Decay (FID) signal, laser power, gas pressure, RGA reading and notifies the operator of the manual steps that need to be taken.

2.7. Measurements

2.7.1. Monitoring polarisation at the filling station and estimating polarisation at the MRI using FID

To monitor the polarising process, Free-Induction-Decay coils [22], one tuned to near ^{129}Xe and the other near the ^{3}He Larmor frequencies in 1 mT, were attached to the OPC. Additional data acquisition hardware and software was used to pulse the coil and measured the FID response. The FID signal provides a relative measurement of the gas polarisation. Data processing has been integrated into the automation control program. We used an average of 200 measurements separated by two

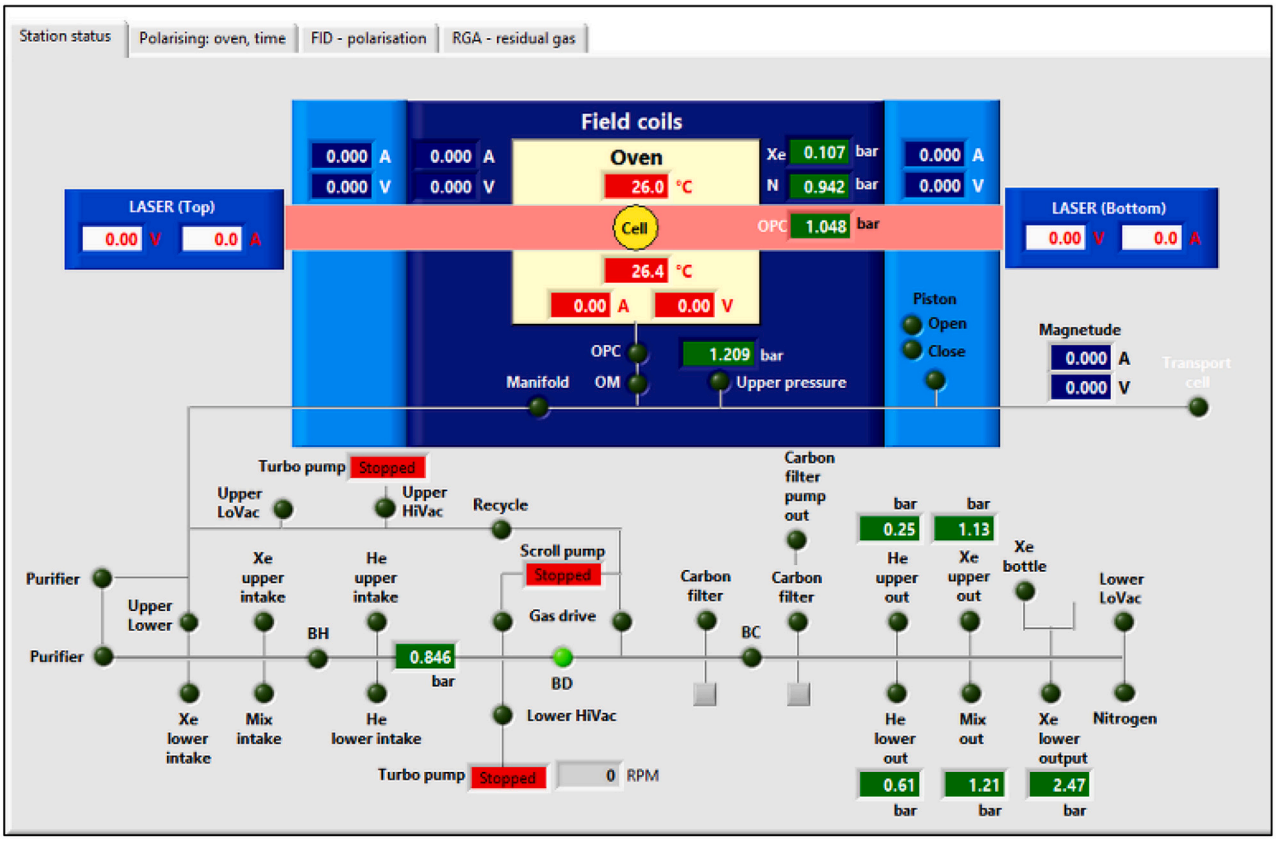

Fig. 5. Control program of the hyperpolariser, showing the system status panel with gas circuit layout, including pneumatic valves, pumps, pressure, temperature, and laser power.

seconds between measurements. A comparison was made for separations of one, two and five seconds between measurements. A drop in signal was consistently observed for one second separation whereas there was virtually no difference in the results with two second separation and with five second separation between measurement.

2.7.2. Magnetic resonance imaging experiments

A Tedlar bag of hyperpolarised ^{3}He gas was generated at Monash Biomedical Imaging and then transported to the Royal Children's Hospital, Melbourne within two hours. An MRI test of the hyperpolarised ^{3}He was performed using a Siemens 3 T scanner (TrioTim, Siemens Medical Solutions, Erlangen, Germany) with a bird-cage ^{3}He lung coil (RAPID Biomedical GmbH, Wuerzburg, Germany) at the Royal Children's Hospital. The resonance frequency of ^{3}He was set to 93.885 MHz. A Flash sequence was used for ^{3}He imaging with the following parameters: flip angle 8^{o}, repetition time 4.6 ms, echo time 2.03 ms, field of view 500 × 500 mm^{2}, matrix size 256 × 256, single slice, and slice thickness 3.3 mm.

For the hyperpolarised ^{129}Xe phantom imaging a 1:4 ratio of enriched xenon (86% ^{129}Xe) and nitrogen was used. After polarising the gas sample for 20–30 min, the gas was transferred to a transport glass cell and then back-filled with nitrogen. The final pressure of the glass cell was 2 bar. The phantom was then taken to the MRI room in a transport cart with uniform magnetic field and immediately placed into the Skyra 3 T MRI at Monash Biomedical Imaging.

For in vivo lamb lung imaging, a glass cell of hyperpolarised ^{129}Xe gas was prepared as above for the 2 bar phantom study. Institutional animal research ethics approval was granted to conduct a pilot study in a preterm lamb model. The lamb was delivered via caesarean section at 128 days gestation (term 149 days), ventilated with pure oxygen and set up in the supine position in the MRI scanner. Before the delivery of the hyperpolarised gas, the ventilator was stopped and pure nitrogen was used to flush the lamb lung. High ^{129}Xe gas was first transferred into a Tedlar bag and then to a 50 ml syringe, this was used to inject about 40 ml of polarised gas into the lamb lung. The piston of the syringe was held to maintain lung inflation during imaging and ventilation was resumed after approximately 30 s.

For the human lung imaging, a Tedlar bag of hyperpolarised ^{129}Xe gas with the same gas mixture as above was prepared in 1 bar. A second bag of pure nitrogen was prepared to reduce the oxygen in lung. A healthy volunteer (male, 39 years old) was internally recruited following receipt of institutional human research ethics approval. The volunteer first inhaled the pure nitrogen and then exhaled as much of the gas as possible. The subject then immediately inhaled the ^{129}Xe gas, indicated to the radiographer to commence imaging, did not breathe during the imaging protocol, and returned to normal respiration after about 15 s.

The MR experiments on the hyperpolarised ^{129}Xe were performed on a Siemens 3 T scanner (Skyra, Siemens Medical Solutions, Erlangen, Germany) with a bird-cage ^{129}Xe lung coil (RAPID Biomedical GmbH, Wuerzburg, Germany) at Monash Biomedical Imaging, Melbourne. The resonance frequency of ^{129}Xe was set to 34.09 MHz. A 2D-GRE sequence was used for ^{129}Xe gas imaging. The phantom image was collected using the following acquisition parameters: flip angle 7°, repetition time 15 ms, echo time 3 ms, field of view 400 × 400 mm^{2}, matrix size 64 × 64, single slice, slice thickness 35 mm, bandwidth 370 Hz/Pixel, and 5 averages. For the in vivo lamb lung imaging experiment, the parameters were: flip angle 7°, repetition time 15 ms, echo time 3 ms, field of view

400 × 400 mm^2, matrix size 64 × 64, single slice, slice thickness 70 mm, bandwidth 370 Hz/Pixel, and 5 averages. For the human lung imaging experiment, the parameters were: flip angle 7°, repetition time 20 ms, echo time 7.81 ms, field of view 500 × 500 mm^2, matrix size 64 × 64, single slice, slice thickness 180 mm, bandwidth 50 Hz/pixel, and 6 averages.

3. Results

In a typical polarising process of ^{129}Xe, every five to ten minutes, ten averages of FID measurements separated by two seconds were automatically done while the laser illuminated the OPC and the temperature was gradually raised to the operational temperature. In our system, when the temperature reached above 80 °C, the FID signal became detectable. The FID signal strength would increase as the ^{129}Xe polarisation increases and plateaued in 10–20 min after the signal was first detected. An FID signal with 100 averages was successfully acquired (Fig. 6). The high number of averages was adopted to provide a high signal-to-noise measurement for illustrative purpose. The FID signal decay time constant T2 = 0.12 s. T2 measures the local magnetic field uniformity. It is comparable to other hyperpolariser. In our measurements, subtracting the FID signal frequency from the FID pulse frequency gave the ^{129}Xe Larmor frequency = 11.822 kHz. The ^{129}Xe Larmor frequency result and the ^{129}Xe gyromagnetic ratio of 11.777 kHz/mT corresponded to a magnetic field slightly more than 1 mT, which is in agreement with the measurement using a magnetic field probe.

MR images of the hyperpolarised gases were successfully acquired for phantom studies, and in lamb and human lung studies. The hyperpolarised ^{3}He gas was imaged in a Tedlar bag with a signal-to-noise ratio (SNR) of approximately three (Fig. 7(a)). The hyperpolarised ^{129}Xe gas was imaged in a pressurised glass cell phantom with a SNR of more than twenty (Fig. 7(b)). Hyperpolarised ^{129}Xe gas was successfully imaging in the lung of a new born lamb (Fig. 7(c)). There was signal loss in the anterior part of the lamb lung (white arrow in Fig. 7(c)). This phenomenon could be also observed in the human lung (see white arrows in Fig. 7(d)). The SNR in the lamb and human lungs were approximately three, which were much lower than observed in the phantom studies.

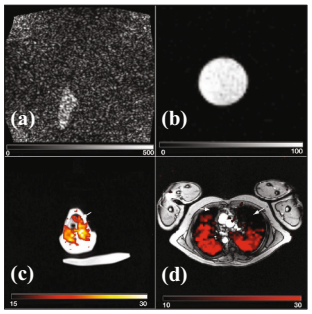

Fig. 7. MR imaging results of (a) hyperpolarised ^{3}He in a Tedlar bag and hyperpolarised ^{129}Xe in a (b) glass cell, (c) *in vivo* lamb lung with signal loss in the anterior part of the lamb lung (white arrow), and (d) in human lung with signal loss also observed in the human lung (white arrows). The image signal intensities are shown in arbitrary units.

4. Discussion

We report the design, construction and initial MR imaging test results of a hyperpolariser for the production of polarised ^{129}Xe and ^{3}He for medical imaging. The hyperpolariser reported herein has several technological advantages and design features, together with a number of operational limitations. A key feature of the system is the use of a Titanium transfer piston. As discussed, the piston effectively separates the OPC from the external transporter and allows more polarised gas to be extracted from the OPC. In our MRI tests, we observed no discernible difference using gas that flowed directly into a transport cell and gas that was transferred through the piston.

Use of a non-inductive electrical heating pad avoids the requirement to circulate hot air that vents into the environment of the hyperpolariser. The Teflon oven however can be improved by using materials with lower thermal conductivity and less thermal mass, such as aerogel with selected thermal characteristics. Not using gas flow can result in up to 20 °C temperature gradient when polarising ^{3}He at about 200 °C. How to reliably generates air flow at this temperature remains to be solved. One important aspect of the heating issue is the use of high-power lasers. The total laser power used in this system is 480 W with about 360 W delivered to the OPC. We have adopted the design from a SEOP system with the same level of laser power that can polarise ^{3}He at a fast rate [10]. However, a key difference of the system is the use of a rubidium

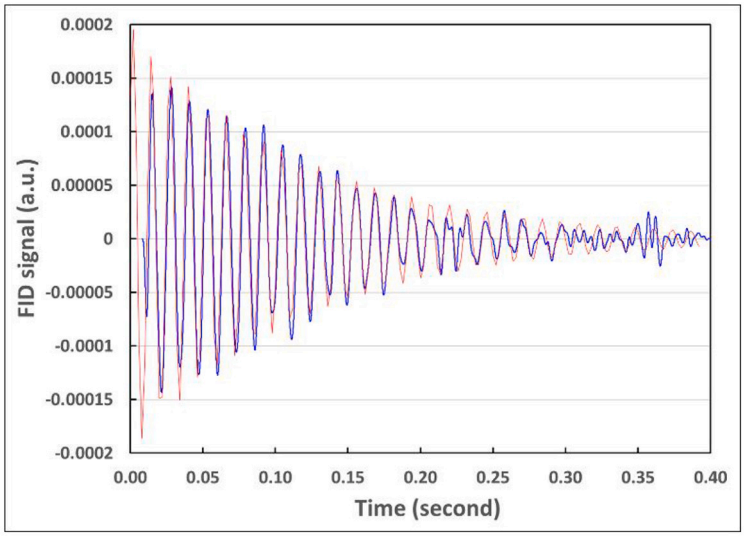

Fig. 6. FID measurement. The FID triggering pulse was 0.8V in amplitude, 11.9 kHz and 5ms long. An average of 200 measurements separated by two seconds between each measurement were taken. The OPC contains 0.5 bar enriched xenon (86% ^{129}Xe) and 1.5 bar nitrogen. The temperature was 85°C in this measurement. The FID signal decay time constant T2=0.12 second. The Lamour frequency of 11.822 kHz corresponded to a field of 1mT.

cell rather than a "hybrid" rubidium-potassium cell. The latter operates at higher temperature but has by design a lower rubidium vapour pressure than a pure rubidium cell. The level of laser power resulted in significant heating of the pure rubidium cell. A small quantity of cooling air over the OPC was needed to prevent it from overheating. We observed that, without cooling air when polarising ^{3}He, the oven temperature stayed at 200 °C due primarily to the laser heating of the OPC but the polarisation decreased. We believe that we have encountered "rubidium runaway" [23]. The compressed air cooling kept the temperature of the oven between 180 °C to 190 °C and as a result, keep the rubidium density at a lower level to prevent rubidium runaway. A further improvement would be the ability to reduce the laser power in the system. When polarising ^{129}Xe at 80 °C to 100 °C, the laser heating did not result in self-sustained heating. The temperature in the oven remained stable under the control of the heater. At that temperature range, the FID signal strength did not vary observably with temperature. When we switched off the heater while keeping the lasers running, the oven temperature gradually dropped to between 60 °C and 70 °C. Beyond 105 °C, the FID signal decreased with increasing temperature. We did not observe rapid temperature excursion up to 120 °C which was the highest temperature in our test. While these observations did not immediately suggest rubidium runaway, they cannot rule out that possibility as the oven temperature may not reflect the temperature variations inside the cell. Observation of the laser transmission profile in the cell would be the definitive determination. However, the use of two-side pumping and an oven with Teflon body and laser transmission windows has prevented us from observing the transmission of the laser through the OPC. A modification of the oven would be needed to allow observations that can determine if there is rubidium runaway.

To carry out the first round of MRI tests with hyperpolarised ^{3}He and ^{129}Xe we used FID to provide a *relative* gas polarisation measurement. Whilst the FID is simple to operate and provides an immediately observable result it is however a relative measurement in hyperpolarization studies due to the sensitivity to small environmental changes. Heating, slight change in positioning relative to the magnetic field, using slightly different field, different FID pulse amplitude and frequency will result in a vastly different FID signal, especially the amplitude of the signal. At the MRI instrument, there is more substantial environmental control to allow FID signal to be reproducible and properly calibrated FID can be explored to provide absolute polarisation measurements. This and other methods to measure absolute polarisation will be the next step that follows this project of hyperpolariser construction and initial MRI evaluation reported here.

The SEOP hyperpolariser was designed to polarise both ^{3}He and ^{129}Xe. Hyperpolarised ^{3}He can provide high spatial resolution for lung imaging [24]. In this study, we demonstrated the capability to produce hyperpolarised ^{3}He for MR imaging. Specially, the gas was generated in one location and imaged in a hospital at another location after approximately two hours. This demonstrates the feasibility to share hyperpolarised ^{3}He for MR lung imaging applications at other sites in the future. Owing to the limited supply of ^{3}He, we did an initial test using hyperpolarised ^{3}He and then undertook multiple experiments using ^{129}Xe. We successfully generated and imaged hyperpolarised ^{129}Xe gas onsite. We achieved high SNR in the phantom, which were similar with the results in [25]. We also achieved in vivo hyperpolarised ^{129}Xe imaging in both lamb and human lungs. Low signal intensities in the anterior part of the lungs were seen in both lamb and human, which is consistent with the gravity-dependent gradient in lung density from anterior to posterior in the supine position [26]. The amplitude of the MR signals in the lamb and the human lungs were lower than observed in the phantom images, possibly because of the negative effects of oxygen in the lung [3].

Hyperpolarised gases suffer from depolarisation caused by oxygen and radio-frequency pulses which reduce the MR signal, this is especially true for xenon imaging where depolarisation is quite rapid [27,28]. For reliable and consistent imaging, it is essential to develop and maintain reliable polarisation percentages and rapid transfer protocols for the delivery of xenon to the MRI scanner suite with minimal interference from magnetic fields and gases which reduce the polarisation. This limits the utility of hyperpolarised xenon for routine clinical imaging as the polariser instrumentation needs to be onsite. Delivery of xenon gas to patients is complex as it is rapidly depolarised by oxygen. Whilst flushing the lungs with nitrogen helps reduce depolarisation this is however not a pleasant experience for patients, especially those with respiratory disease. Proper processes for reliable delivery of hyperpolarised gas into patients with respiratory diseases requires further development.

While the main goals to demonstrate production of hyperpolarised ^{129}Xe and ^{3}He and to obtain MRI measurements were achieved, the hyperpolariser is far from optimal and can be further improved. Future work will thoroughly and systemically map the operational parameters of the hyperpolariser in order to improve the performance, similar to the process reported in reference [12]. T1 measurements of the key components and absolute polarisation measurements at the hyperpolariser and the MRI will be performed using published methods to measure the absolute polarisation. We also plan to compare the FID signal of a cell of polarised ^{129}Xe with the FID signal of the Boltzmann polarisation of unpolarised ^{129}Xe in the same cell in the MRI, based on the fact that the MRI is a more stable magnetic environment for measurement of the FID signal reproducibility. For measurements during optical pumping, a technique called electron paramagnetic resonance frequency (EPR) shift has been proven to work [29]. The method monitors the EPR shift of alkali atoms in the presence of the nuclear-polarised noble gas. We intend to implement this as the next step in further optimisation and improvement of the hyperpolariser. In addition, polarised gas extraction using the piston can work well with a liquid nitrogen cold trap to freeze and collect polarised ^{129}Xe in a Halbach cylinder. This will enable optimal extraction of the ^{129}Xe gas with preservation of the polarisation. The increase of polarisation lifetime to a few hours will also allow several cycles of polarised gas production to be carried out, increasing the amount of polarised ^{129}Xe delivered to the application.

5. Conclusion

We report the design, construction and MR imaging test results of a hyperpolariser for the production of polarised ^{129}Xe and ^{3}He for medical imaging. Consistent with the continuous improvement of hyperpolariser technologies by many groups over the decades, the system has incorporated several technological improvements that build upon existing hyperpolariser designs. Initial tests have been successfully performed to obtain MRI images of ^{129}Xe in animal and human lungs. This work serves as a starting point at our centre to develop the methodologies of medical imaging with hyperpolarised gas and to undertake further improvements in the design of hyperpolariser for medical imaging use.

Acknowledgements

We would like to acknowledge support from the Australian Research Council (Grant LE130100035) for funding to construct the hyperpolariser, the National Health and Medical Research Council (Grant APP606944), and CASS foundation (Grant SM/14/5587) for funding to support use of the hyperpolariser. The authors would like to acknowledge the Australian National Imaging Facility, a national collaborative research infrastructure scheme (NCRIS) capability at Monash Biomedical Imaging for contributions to the facilities, technical expertise and for fellowships to GZ and MdV.

[1–29] References

[1] Petersen E, Koopmans M, Go U, Hamer DH, Petrosillo N, Castelli F, et al. Comparing SARS-CoV-2 with SARS-CoV and influenza pandemics. Lancet Infect. Dis. 2020;20:e238–44. https://doi.org/10.1016/S1473-3099(20)30484-9.

[2] Zhao YM, Shang YM, Song WB, Li QQ, Xie H, Xu QF, et al. Follow-up study of the pulmonary function and related physiological characteristics of COVID-19 survivors three months after recovery. Clin Med 2020;20:100463. https://doi.org/10.1016/j.eclinm.2020.100463.
[3] Mugler JP, Altes TA. 129Xe MRI of the human lung. J. Magn. Reson. Imaging 2013;37:313–31. https://doi.org/10.1002/jmri.23844.
[4] Albert MS, Cates GD, Driehuys B, Happer W, Saam B, Springer CS, et al. Biological magnetic resonance imaging using laser-polarized 129Xe. Nature 1994;370(6486):199–201. https://doi.org/10.1038/370199a0.
[5] MacFall JR, Charles HC, Black RD, Middleton H, Swartz JC, Saam B, et al. Human lung air spaces: potential for MR imaging with hyperpolarized He-3. Radiology 1996;200(2):553–8. https://doi.org/10.1148/radiology.200.2.8685356.
[6] Touchiat M, Carver TR, Varnum CM. Nuclear polarization in 3He gas induced by optical pumping and dipolar exchange. Phys. Rev. Lett. 1960;5:573. https://doi.org/10.1103/PhysRevLett.5.373.
[7] Walker TG, Happer W. Spin-exchange optical pumping of noble-gas nuclei. Rev. Mod. Phys. 1997;69:629. https://doi.org/10.1103/RevModPhys.69.629.
[8] Thien F, Friese M, Cowin G, Maillet D, Wang D, Galloway G, et al. Feasibility of functional magnetic resonance lung imaging in Australia with long distance transport of hyperpolarized helium from Germany. Respirology 2008;13(4):599–602. https://doi.org/10.1111/j.1440-1843.2008.01262.x.
[9] Batz M, Nacher PJ, Tastevin G. Fundamentals of metastability exchange optical pumping in helium. J. Phys. Conf. Ser. 2011;294:012002. https://doi.org/10.1088/1742-6596/294/1/012002.
[10] Lee WT, Tong X, Pierce J, Fleenor M, Ismaili A, Robertson JL, et al. In-situ polarized 3He-based neutron polarization analyzer for SNS magnetism reflectometer. J. Phys. Conf. Ser. 2010;251:012086. https://doi.org/10.1088/1742-6596/251/1/012086.
[11] Nikolaou P, Coffey AM, Walkup LL, Gust BM, Whiting N, Newton H, et al. XeNA: an automated 'open-source' (129)Xe hyperpolarizer for clinical use. Magn. Reson. Imaging 2014;32(5):541–50. https://doi.org/10.1016/j.mri.2014.02.002.
[12] Nikolaou P, Coffey AM, Walkup LL, Gust BM, Whiting N, Newton H, et al. Near-unity nuclear polarization with an open-source 129Xe hyperpolarizer for NMR and MRI. PNAS 2013;110(35):14150–5. https://doi.org/10.1073/pnas.1306586110.
[13] Klimcak CM, Huang M, Camparo JC. Alkali metal consumption by discharge lamps fabricated from GE-180 aluminosilicate glass. In: 2015 Joint Conference of the IEEE International Frequency Control Symposium & the European Frequency and Time Forum. CO: Denver; 2015. p. 180–7. https://doi.org/10.1109/FCS.2015.7138818.
[14] Sakaguchi Y, Kira H, Oku T, Shinohara T, Suzuki J, Sakai K. Structure of glasses for 3He neutron spin filter cells. J. Phys. Conf. Ser. 2011;294:012004. https://doi.org/10.1088/1742-6596/294/1/012004.
[15] Lee WT, Tong X, Rich D, Liu Y, Fleenor M, Ismaili A, et al. Increasing the pump-up rate to polarize 3He gas using spin-exchange optical pumping method. Physica B 2009;404:2670–2. https://doi.org/10.1016/j.physb.2009.06.037.
[16] Whiting N, Nikolaou P, Eschmann NA, Goodson BM, Barlow MJ. Interdependence of in-cell xenon density and temperature during Rb/129Xe spin-exchange optical pumping using VHG-narrowed laser diode arrays. J. Magn. Reson. 2011;208(2):298–304. https://doi.org/10.1016/j.jmr.2010.11.016.
[17] Nikolaou P, Coffey AM, Ranta K, Walkup LL, Gust BM. BarlowMJ. Multidimensional mapping of spin-exchange optical pumping in clinical-scale batch-mode 129Xe hyperpolarizers. J. Phys. Chem. B 2014;118(18):4809–16. https://doi.org/10.1021/jp501493k.
[18] Tong X, Pierce J, Lee WT, Fleenor M, Chen WC, Jones GL, et al. Electrical heating for SEOP-based polarized 3He system. J. Phys. Conf. Ser. 2010;251:012087. https://doi.org/10.1088/1742-6596/251/1/012087.
[19] Nikolaou P, Whiting N, Eschmann NA, Chaffee KE, Goodson BM, Barlow MJ. Generation of laser-polarized xenon using fiber-coupled laser-diode arrays narrowed with integrated volume holographic gratings. J. Magn. Reson. 2009;197:249–54. https://doi.org/10.1016/j.jmr.2008.12.015.
[20] Gottardi G, Mesirca P, Agostini C, Remondini D, Bersani F. A four coil exposure system (tetracoil) producing a highly uniform magnetic field. Bioelectromagnetics 2003;24:125–33. https://doi.org/10.1002/bem.10074.
[21] Becker J, Heil W, Krug B, Leduc M, Meyerhoff M, Nacher PJ. Study of mechanical compression of spin-polarized 3He gas. Nucl Instrum Methods Phys Res A 1994;346(1–2):45–51. https://doi.org/10.1016/0168-9002(94)90687-4.
[22] Parnell SR, Woolley EB, Borg S, Frost CD. Digital pulsed NMR spectrometer for nuclear spin-polarized 3He and other hyperpolarized gases. Meas. Sci. Technol. 2008;19:045601. https://doi.org/10.1088/0957-0233/19/4/045601.
[23] Witte C, Kunth M, Rossella F, Schröder L. Observing and preventing rubidium runaway in a direct-infusion xenon-spin hyperpolarizer optimized for high-resolution hyper-CEST (chemical exchange saturation transfer using hyperpolarized nuclei) NMR. J. Chem. Phys. 2014;140:084203. https://doi.org/10.1063/1.4865944.
[24] Wild JM, Paley MN, Viallon M, Schreiber WG, van Beek EJ, Griffiths PD. K-space filtering in 2D gradient-echo breath-hold hyperpolarized 3He MRI: spatial resolution and signal-to-noise ratio considerations. Magn. Reson. Med. 2002;47(4):687–95. https://doi.org/10.1002/mrm.10134.
[25] Zhao L, Mulkern R, Tseng CH, Williamson D, Patz S, Kraft R, et al. Gradient-echo imaging considerations for hyperpolarized 129Xe MR. J Magn Reson B 1996;113:179–83. https://doi.org/10.1006/jmrb.1996.0173.
[26] Qing K, Ruppert K, Jiang Y, Mata JF, Miller GW, Shim YM, et al. Regional mapping of gas uptake by blood and tissue in the human lung using hyperpolarized xenon-129 MRI. J. Magn. Reson. Imaging 2014;39:346–59. https://doi.org/10.1002/jmri.24181.
[27] Dregely I, Ruset IC, Wiggins G, Mareyam A, Mugler JP, Altes TA, et al. A 32-channel phased-array receive with asymmetric birdcage transmit coil for hyperpolarized xenon-129 lung imaging. Magn. Reson. Med. 2013;70(2):576–83. https://doi.org/10.1002/mrm.24482.
[28] Doganay O, Matin TN, Mcintyre A, Burns B, Schulte RF, Gleeson FV, et al. Fast dynamic ventilation MRI of hyperpolarized 129Xe using spiral imaging. Magn. Reson. Med. 2018;79(5):2597–606. https://doi.org/10.1002/mrm.26912.
[29] Schaefer SR, Cates GD, Chien TR, Gonatas D, Happer W, Walker TG. Frequency shifts of the magnetic-resonance spectrum of mixtures of nuclear spin-polarized noble gases and vapors of spin-polarized alkali-metal atoms. Phys. Rev. A 1989;39:5613. https://doi.org/10.1103/PhysRevA.39.5613.